Dynamic Response Analysis of Three Floating Wind Turbine Concepts with a Two-Bladed Darrieus Rotor

Zhengshun Cheng[1], Kai Wang[2], Zhen Gao[1], Torgeir Moan[3]

1 Department of Marine Technology, Norwegian University of Science and Technology, Trondheim, Norway
2 Centre for Ships and Ocean Structures (CeSOS), Norwegian University of Science and Technology, Trondheim, Norway
3 Centre for Autonomous Marine Operations and Systems (AMOS), Norwegian University of Science and Technology, Trondheim, Norway

Recently, interest in the development of floating vertical axis wind turbines (FVAWTs) has been increasing, since FVAWTs might prove to be one of the optimal configurations in deep waters. In this study, a FVAWT with a 5 MW Darrieus rotor was used as the reference wind turbine and was mounted on three different floating support structures: the OC3 spar buoy, the OC4 semi-submersible, and a tension leg platform (TLP). Fully coupled nonlinear time domain simulations using the code SIMO-RIFLEX-DMS were conducted. A series of load cases with turbulent wind and irregular waves was carried out to investigate the dynamic responses of these three FVAWT concepts by estimating the generator power production, the platform motions, the tower base bending moments, and the mooring line loads. For the spar, semi-submersible, and TLP FVAWT concepts, twice-per-revolution (2P) effects resulting from the 2P aerodynamic loads are prominent in the dynamic responses of these concepts. Because of the compliant catenary mooring systems, the spar and the semi-submersible can help to mitigate the 2P effects on structural loads and mooring line tensions as compared to the TLP concept, at the cost of larger platform motions. The TLP is not a good substructure for a vertical axis wind turbine unless the cyclic variation of aerodynamic loads is significantly reduced.

KEY WORDS: Floating vertical axis wind turbine, dynamic analysis, spar; semi-submersible, tension leg platform.

INTRODUCTION

During the 1970s and 1980s, considerable efforts were devoted to investigate and develop Darrieus vertical axis wind turbines (VAWTs), mainly in the USA and Canada (Paraschivoiu, 2002). Commercial Darrieus VAWTs were also developed by the FloWind Corporation. Unfortunately, after the bankruptcy of the FloWind Corporation and the termination of VAWT research sponsored by the U.S. Department of Energy, VAWTs lost ground to the horizontal axis wind turbines (HAWTs) that are predominant today. However, as wind farms are moving toward deeper waters where large floating wind turbines will be more economical, this may change, since the cost of installation and maintenance will become relatively more important.

As a matter of fact, floating vertical axis wind turbines (FVAWTs) have several advantages over floating horizontal axis wind turbines (FHAWTs), such as lower centers of gravity, wind direction independence, and lower costs. Paquette and Barone (2012) indicated that FVAWTs have the potential of achieving more than 20% of the cost of energy reductions compared with FHAWTs. Moreover, FVAWTs are more suitable for deployment as wind farms compared to FHAWTs. The wake of a pair of counter-rotating H-rotors can dissipate much more quickly than that of FHAWTs, allowing them to be packed closer (Kinzel et al., 2012). The average power generated by a pair of H-rotors at all azimuth angles is higher than that of an isolated turbine (Dabiri, 2011), implying that the conversion efficiency of VAWTs can be improved. In addition, other efforts on comparative study of HAWTs and VAWTs have also been made by several researchers to reveal the merits and feasibilities of each concept, including Paraschivoiu (2002), Islam et al. (2013), and Jamieson (2011). Borg et al. (2014) compared VAWTs with HAWTs in technology, conversion efficiency, upscaling, fatigue, machinery position, etc. Wang et al. (2014) conducted a comparative study of a FVAWT with a 5 MW Darrieus rotor (Vita, 2011) and a FHAWT with the NREL 5 MW wind turbine (Jonkman et al., 2009), both mounted on the OC4 semi-submersible platform (Robertson et al., 2012).

For these reasons, an interest in FVAWTs is resurging, and various FVAWT concepts are being proposed, including the DeepWind concept (Paulsen et al., 2011), VertiWind concept (Cahay et al., 2011), etc. Similar to those of the FHAWTs, the substructures for the FVAWT concepts can also be classified into the spar, semi-submersible, and tension leg platform (TLP) types in terms of how they achieve static stability. A semi-submersible type FVAWT with a 5 MW Darrieus rotor mounted on the OC4 DeepCwind semi-submersible (Robertson et al., 2012) was proposed and analyzed by Wang et al. (2013). A spar type FVAWT with the same rotor placed on the OC3 Hywind spar buoy (Jonkman, 2010) was also put forward by Borg and Collu (2014) and Cheng et al. (2015). Fully coupled aero-hydro-servo-elastic dynamic simulations were carried out for the FVAWTs. State-of-the-art limited comparative studies on different FVAWT concepts have been

conducted. Borg and Collu (2014) performed preliminary investigations of the dynamic responses of FVAWTs with the spar, semi-submersible, and TLP floaters; however, the yaw of the spar and the surge and sway of the TLP were disabled during the simulations. Moreover, the structural elasticity and variable speed control were not taken into account.

To better understand the performance and benefit of FVAWTs, the current work compares the dynamic response characteristics of three FVAWT concepts. A 5 MW Darrieus rotor was mounted on three platforms: the OC3 Hywind spar (Jonkman, 2010), the OC4 DeepCwind semi-submersible (Robertson et al., 2012), and a TLP design by Bachynski and Moan (2012). Fully coupled time domain simulations were carried out using the SIMO-RIFLEX-DMS code, which is an aero-hydro-servo-elastic computational code. A number of load cases (LCs) were carried out to study the dynamic responses of the three FVAWT concepts. Motions, tower base bending moments, and mooring line tensions were calculated and compared. The results reveal the merits, disadvantages, and feasibilities of each FVAWT concept and will help to resolve preliminary design trade-offs among the three FVAWT concepts.

FLOATING WIND TURBINE MODELS

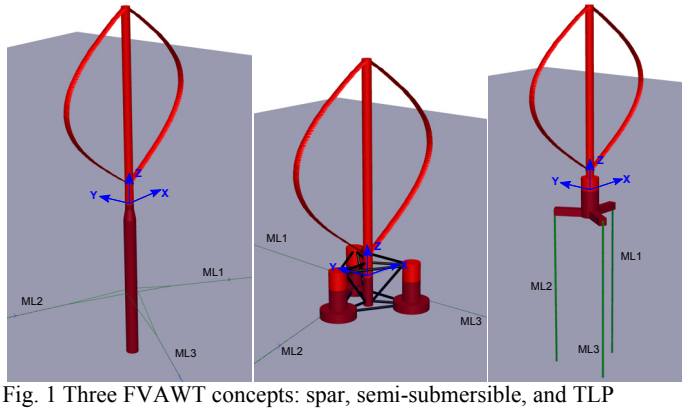

Fig. 1 Three FVAWT concepts: spar, semi-submersible, and TLP

Three floating support structures were studied here: namely a spar, a semi-submersible, and a TLP, as depicted in Fig. 1 and listed in Table 2. The concepts were used to support a 5 MW Darrieus rotor, which is the baseline design developed in the DeepWind project (Vita, 2011). The rotor is comprised of two blades and one rotating tower that spans from the top to the bottom, which is connected to the generator. Main specifications of this rotor are summarized in Table 1. The generator considered here was assumed to be placed at the tower base, and the generator mass was incorporated in the platform hull mass.

The concepts were originally designed to support the NREL 5 MW wind turbine (Jonkman et al., 2009). The concepts were considered in the water depth where they were designed, ranging from 150 m for the TLP to 200 m for the semi-submersible to 320 m for the spar. Here reasonable modifications were made to each platform to support the 5 MW Darrieus rotor, such as adjusting the ballast of the spar and the semi-submersible, and the tendon pre-tension of the TLP. For each platform, the draft and displacement were maintained the same as the original one. Since the difference in mass between the 5 MW Darrieus rotor and the NREL 5 MW wind turbine was small compared to the displacements of the three concepts, it was assumed that such modifications would not alter the hydrostatic performance of each platform significantly, which was verified by the following simulations.

After these modifications, these substructures supporting the 5 MW Darrieus rotor may not be optimal from an economical point of view, but they are sufficient to demonstrate the inherent motion and structural response characteristics of each concept.

Rated power [MW]	5
Rotor height, root to root [m]	129.56
Rotor radius [m]	63.74
Chord length [m]	7.45
Airfoil section	NACA 0018
Cut-in, rated, cut-out wind speed [m/s]	5 , 14 , 25
Rated rotational speed [rpm]	5.26
Total mass, including rotor and tower [kg]	754,226
Center of mass [m]	(0 , 0 , 75.6)

Table 1 Specifications of the Darrieus 5 MW wind turbine

Floater	Spar	Semi	TLP
Water depth [m]	320	200	150
Draft [m]	120	20	22
Waterline diameter [m]	6.5	12.0/6.5	14.0
Hull mass, including ballast and generator [ton]	7,308.3	13,353.7	2,771.9
CM location below MSL [m]	–89.76	–13.42	–15.38
Displacement [m^3]	8,027	13,919	5,655
CB location below MSL [m]	–62.06	–13.15	–14.20
Moment of inertia in roll about global x-axis [ton·m^2]	6.362×10^7	9.159×10^6	9.871×10^5
Moment of inertia in pitch about global y-axis [ton·m^2]	6.362×10^7	9.159×10^6	9.871×10^5
Moment of inertia in yaw about platform centerline [ton·m^2]	1.588×10^5	1.209×10^7	2.288×10^5

Table 2 Properties of the three floating platforms; MSL, mean sea level; CM, center of mass; CB, center of buoyancy.

Spar Structure

The spar platform studied here was the OC3 Hywind hull, as described by Jonkman (2010). The spar consists of two cylindrical regions connected by a linearly tapered conical region. The heavy ballast located at the bottom provides good stability and restoring stiffness, thus limiting the platform pitch and roll motion in wind and waves. A catenary chain mooring system with delta lines and clump weights was applied to approximate the horizontal restoring stiffness as described by Jonkman (2010); a schematic layout of the mooring system is illustrated by Karimirad and Moan (2012). Because of the difference in mass between the Darrieus rotor and the NREL 5 MW wind turbine, the ballast was adjusted to retain the same draft and displacement specified for the spar FHAWT, leading to changes in the hull mass, center of gravity, and moment of inertia, as highlighted in Table 2. The moments of inertia are calculated with respect to the origin of the global coordinate system, as shown in Fig. 1.

Semi-Submersible Structure

The semi-submersible platform considered here was the OC4

DeepCwind semi-submersible, as defined by Robertson et al. (2012). The semi-submersible is composed of three offset columns, three pontoons, a central column, and braces. The rotor is located on the central column. Braces are used to connect all of the columns as an integrated body. Three catenary mooring lines are attached to the three offset columns to provide horizontal restoring stiffness. Good stability is achieved by the large waterplane area moment of inertia to limit the pitch and roll motion in wind and waves. The ballast was also adjusted to maintain the same draft and displacement as that of the semi-submersible FHAWT described by Robertson et al. (2012).

Tension Leg Structure

The TLP model considered here was a design by Bachynski and Moan (2012), which is identical to the TLPWT 3. The TLP model consists of one large central column, which contributes to approximately 60% of the displacement, and three pontoons. The stability is obtained by three tendons to limit the global motions in wind and waves. Because of the tendon pretension, the hull mass, including ballast and generator, is approximately one-half of that corresponding to the displacement, as shown in Table 2. Here the same draft and displacement as the TLP FHAWT were also maintained for the TLP FVAWT by changing the tendon pre-tension from 8,262 kN to 7,450.9 kN.

METHODOLOGY

Numerical simulations were carried out in order to investigate the dynamic responses of the FVAWTs. The code SIMO-RIFLEX-DMS, developed by Wang et al. (2013; 2015a), was used to conduct the fully coupled nonlinear time domain simulations. It can account for the turbulent wind inflow, aerodynamics, hydrodynamics, control dynamics, structural mechanics, and mooring line dynamics. Three computer codes are integrated in the code SIMO-RIFLEX-DMS. SIMO computes the rigid body hydrodynamic forces and moments on the hull (MARINTEK, 2012a); RIFLEX represents the blades, tower, shaft, and mooring lines as nonlinear bar or beam elements and provides the links to an external controller and DMS (MARINTEK, 2012b); and DMS calculates the aerodynamic loads on the rotor. The generator torque controller was written in Java, which is able to maximize the power capture below the rated operating point and keep the rotational speed constant above the rated operating point. The SIMO-RIFLEX wind turbine module has previously been verified (Luxcey et al., 2011; Ormberg et al., 2011) and the code SIMO-RIFLEX-DMS was verified in Wang et al. (2013).

The aerodynamic loads on the rotor were calculated according to the double multi-streamtube (DMS) theory (Paraschivoiu, 2002). The DMS model accounted for the effect of variation in the Reynolds number and incorporated the effect of dynamic stall using the Beddoes--Leishman dynamic stall model. In the DMS model, the relative velocity seen at a blade section is the vector sum of the free wind speed, the induced velocity, subtracting the velocity due to the motion. The velocity of the motion is comprised of the blade rotation, the translational and rotational velocities of the platform, and the elastic deformation of the blades. The aerodynamic code DMS is validated by comparison with experimental results (Wang et al., 2015a).

The hydrodynamic model of each concept included a combination of potential flow and Morison's equation. Added mass, radiation damping and first order wave forces were obtained from a potential flow model and applied in the time domain using the convolution technique (Faltinsen, 1995). Additional viscous forces on large volume structures were incorporated through the Morison equation. The Morison equation was also applied to slender elements that were not included in the potential flow model. Morison coefficients in the hydrodynamic model are those used by Bachynski et al. (2014). In addition to the first-order and viscous hydrodynamic forces, second-order wave forces were also considered for the spar, semi-submersible, and TLP, respectively. For the spar hull, the mean wave drift forces were applied, and Newman's approximation was used to estimate the second-order difference-frequency wave excitation forces. Regarding the semi-submersible platform, the second-order difference-frequency wave excitation force was considered, using the full quadratic transfer function (QTF). The effect of second-order difference-frequency force on the dynamic responses of this semi-submersible FVAWT in misaligned wind--wave conditions was studied by Wang et al. (2015c). With respect to the TLP FVAWT, second-order difference-frequency wave excitation forces using Newman's approximation and sum-frequency wave excitation forces using the full QTF were applied.

Regarding the structural model of each concept, the platform hull was considered as a rigid body. The tower, blades, and shaft were modeled by using beam elements; the catenary mooring lines of the spar and semi-submersible were represented by using bar elements; and the tendons for the TLP were modeled by using beam elements and connecting joints.

LOAD CASES (LCs) AND ENVIRONMENTAL CONDITIONS

A series of load cases (LCs) was defined to perform the comparative study for the three FVAWT concepts, as summarized in Tables 3 and 4. In LC1, free decay tests in surge, heave, pitch, and yaw were carried out to assess the natural periods. In LC2, both the unidirectional white noise test and a number of regular wave tests were conducted to estimate the response amplitude operators (RAOs) of the FVAWTs. In LC3 are six conditions with correlated and directionally aligned wind and waves.

	Load cases (LCs)	Response	Wind	Waves
LC1	Decay	Decay	–	Calm water
LC2.1	White noise	RAO	–	White noise
LC2.2	Regular waves	RAO	–	Regular waves

Table 3 Load cases (LCs): decay, white noise, and regular wave conditions

LC	U_w [m/s]	H_s [m]	T_p [s]	Turb. Model	Sim. Len. [s]
LC3.1	5	2.10	9.74	NTM	3,600
LC3.2	10	2.88	9.98	NTM	3,600
LC3.3	14	3.62	10.29	NTM	3,600
LC3.4	18	4.44	10.66	NTM	3,600
LC3.5	22	5.32	11.06	NTM	3,600
LC3.6	25	6.02	11.38	NTM	3,600

Table 4 Load cases (LCs): combined wind and wave conditions; NTM, normal turbulence model; Sim. Len. simulation length.

The three-dimensional turbulent wind fields were generated by using the National Renewable Energy Laboratory's (NREL's) TurbSim program (Jonkman, 2009) according to the Kaimal turbulence model for IEC Class C. Both the normal wind profile (NWP) and normal turbulence model (NTM) were applied. Regarding the NWP condition, the wind profile $U(z)$ is the average wind speed as a function of height z above the mean sea level (MSL) and is given by the power law as follows:

$$U(z) = U_{\text{ref}}(z/z_{\text{ref}})^{\alpha} \quad (1)$$

where U_{ref} is the reference wind speed, z_{ref} is the height of the reference wind speed, and α is the power law exponent. The value of z_{ref} was set to 79.78 m (the vertical center of the blades) above the MSL. The value of α was chosen to be 0.14 for the floating wind turbines according to IEC 61400-3 (IEC, 2009). The mean wind speed U_w given in Table 4 is the reference wind speed at the vertical center of the blades. The JONSWAP wave model was used to generate the wave history. The significant wave height H_s and peak period T_p were set in accordance with the correlation with wind speed for the Statfjord site in the northern North Sea (Johannessen et al., 2002).

For the combined wind and wave simulations, each simulation lasted 4,600 s and corresponded to a one-hour dynamic analysis, since the first 1,000 s were removed to eliminate the start-up transient effects. Five identical and independent one-hour simulations with different seeds for the turbulent wind and irregular waves were carried out for each LC to reduce the stochastic variations. It should be noted here that only LC3.2 and LC3.3 were conducted for the TLP FVAWT, since negative tendon axial forces will arise for large wind speeds. One possible reason for such negative tendon tension is due to the reduction of tendon pre-tension, but the primary reason is due to the essential characteristics of aerodynamic loads acting on the rotor. The aerodynamic loads are always periodic and are varying with large amplitude, which induce a twice-per-revolution (2P) response in platform motions and thus cause large variation of tension in the tendon, as demonstrated in Fig. 6. Figure 2 also presents the time history of the tendon axial force for the TLP FVAWT in LC3.3. Large variations are observed in the tendon axial forces with period equal to the 2P period. These variations increase with increasing mean wind speed and give rise to negative axial forces, which is unrealistic.

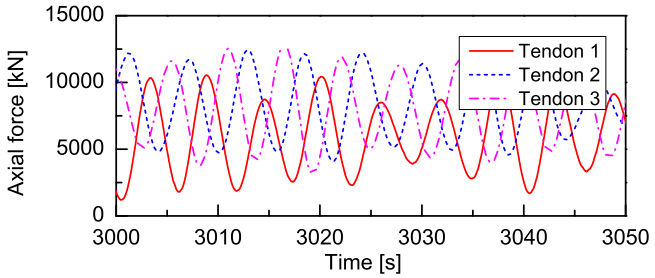

Fig. 2 Time history of the tendon axial forces for the TLP FVAWT in LC3.3 with U_w=14 m/s, H_s=3.62 m, and T_p=10.29 s

RESULTS and DISCUSSIONS

Free Decay Tests

The three floaters considered here are originally designed to support the NREL 5 MW baseline wind turbine. When they are used to support the 5 MW Darrieus rotor, modifications such as adjusting the ballast for the spar and the semi-submersible or reducing the tendon pre-tension for the TLP have been made to maintain the same draft and displacement as the original ones. Such modifications can lead to changes in the natural periods in the global motions. The natural periods of the three FVAWT concepts are given in Table 5. Free decay tests in calm water were carried out to estimate the natural periods. In the free decay tests, the wind turbine was parked with the rotor plane parallel to the x-axis of the global coordinate system as demonstrated in Fig. 1, and no aerodynamic loads acted on the rotor.

In surge and sway, the spar and the semi-submersible have very large natural periods because of the relatively small surge and sway restoring stiffness of the catenary mooring system employed. In heave, the natural periods of the spar and the TLP are located outside the upper and lower limits of ocean wave periods, respectively, while the natural period of the semi-submersible is well within the wave excitation range, indicating that significant heave motion for the semi-submersible can be excited. In roll and pitch, the natural periods of these three platforms are also well situated outside the wave periods, implying that the wave-induced pitch motion will be small. In addition, for the TLP FVAWT, due to the rotor orientation, the rotor contributes a lot to the roll/pitch moments of inertia and causes different roll and pitch natural periods. Since the yaw natural period of the spar is well within the wave period, the spar FVAWT may experience significant yaw motion.

Floater	Spar	Semi	TLP
Surge/Sway [s]	130.8	114.0	45.3
Heave [s]	27.3	17.1	0.6
Roll/Pitch [s]	34.5	31.0	4.5/4.9
Yaw [s]	8.5	79.7	19.3

Table 5 Natural periods of the three FVAWT concepts obtained by free decay tests

Response Amplitude Operators (RAOs) for Wave Loads

The hydrodynamic performance of the three floating concepts can be characterized by response amplitude operators (RAOs). The RAOs can be obtained through unidirectional white noise simulations or a number of regular wave simulations. In the present study both white noise simulations and regular wave simulations were performed. The white noise waves were generated using fast Fourier transform (FFT) with a frequency interval $\Delta\omega = 0.005$ rad/s. The surge and pitch RAOs are presented in Figs. 3 and 4, respectively. The white noise simulation technology captures almost the same natural frequencies as those obtained by the free decay tests. It also predicts all RAOs accurately except at the resonant frequency of each mode. Since the center of gravity of the spar FVAWT is approximately 73.5 m below MSL, there is a close coupling between surge and pitch, resulting in relatively large surge RAOs at the pitch natural frequency, as illustrated in Fig. 3. As given in Table 5 and demonstrated in Figs. 3 and 4, the natural frequencies of surge and pitch for the spar FVAWT and the semi-submersible FVAWT are very close to each other. In addition, the semi-submersible FVAWT has much larger RAOs at both surge and pitch resonant frequencies than the spar FVAWT. Regarding the TLP FVAWT, it only exhibits large surge RAOs in the vicinity of the surge natural frequency, and the pitch RAOs are very close to zero as a result of the tensioned tendons.

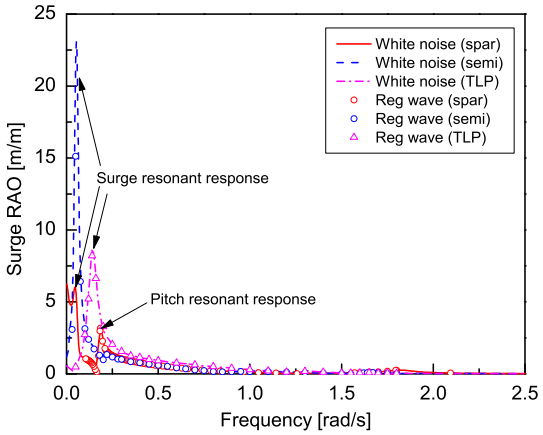

Fig. 3 Surge RAO of the three FVAWT concepts

During the present simulations, the structural elasticity of the curved blades and the tower were taken into account. Peaks corresponding to the elastic blade flatwise mode are thus observed in the pitch RAO for the spar FVAWT and the semi-submersible FVAWT, as presented in Fig. 4. The first 10 eigen modes of the onshore VAWT have been discussed by Wang et al. (2013). It is obvious that the first blade flatwise frequency and the frequencies corresponding to these two peaks for the spar FVAWT and the semi-submersible FVAWT do not exactly coincide. These discrepancies come from the differences in mass and restoring coefficients of the floating platforms, which cause a small shift in the first blade flatwise frequency as compared to the onshore VAWT.

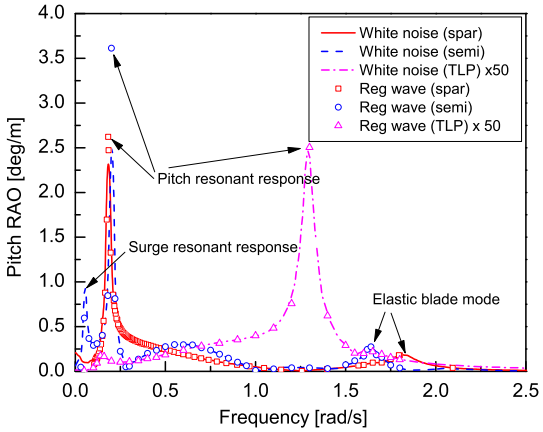

Fig. 4 Pitch RAO of the three FVAWT concepts; the pitch RAO of the TLP FVAWT is multiplied by 50

Generator Power Performance

The stochastic dynamic responses of the three FVAWT concepts are studied under the turbulent wind and irregular wave conditions, including the generator power production, global platform motion, tower base fore-aft and side-to-side bending moment, and the tensions of the mooring lines. For each case of each FVAWT model, five identical and independent one-hour simulations were performed; the mean value and standard deviation of the dynamic responses were obtained by averaging the mean values and standard deviations of five one-hour ensembles.

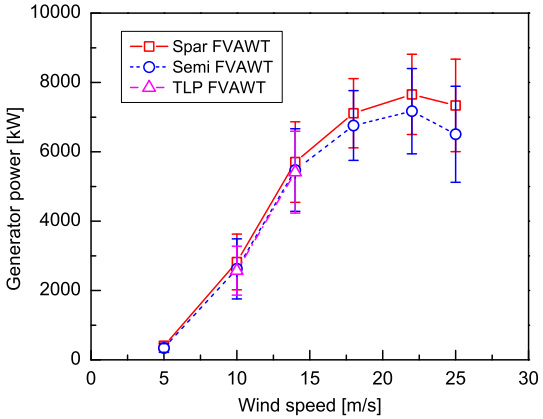

Fig. 5 Mean power production for the three FVAWT concepts with error bar indicating the standard deviation from the mean value

Figure 5 shows the generator power production of the three FVAWT concepts under the turbulent wind and irregular wave conditions. Hereinafter the results are plotted with the mean wind speed as the variable along the abscissa axis for simplicity. The power curve is based on the mean generator power production with the error bar showing the standard deviation from the mean value. The mean generator powers of the three FVAWT concepts increase as the wind speed increases. At rated wind speed of 14 m/s, the mean generator powers slightly exceed the rated power of 5 MW, since the Beddoes--Leishman dynamic stall model is included in the DMS model. The controller implemented is designed to keep the rotational speed constant when the rated operating point is reached; the mean generator powers are therefore increasing at above rated wind speeds. The effects of this nonconstant power production at above rated wind speeds on the grid can be reduced when the FVAWTs are operated as wind farms. Moreover, a more robust controller will be developed in the future to improve the generator power performance for the FVAWT.

In addition, the mean generator powers of the three FVAWT concepts are very close to each other, except at high wind speeds where the mean generator power of the semi-submersible FVAWT begins to differ from that of the spar FVAWT. The difference results from the different rotational speed and increases as the wind speed increases. The different rotational speed for the three concepts is due to the fact that the controller implemented in the present study is not very robust: it fails to keep the rotational speed at above rated wind speed exactly constant. The variations of the generator power for the three FVAWT concepts are very close to each other as well.

Platform Motions

Because of the differences in structural and hydrodynamic properties and in mooring systems, the three FVAWT concepts present different global motions. The platform motions are defined in the global coordinate system with the z-axis along the tower and the x-axis parallel to the wind direction, as depicted in Fig. 1. Power spectra analysis with frequency smoothing using a Parzen window function was used to analyze the time series of global motions. Figure 6 shows the power spectrum of surge, roll, pitch, and yaw motions for the three FVAWT concepts under the turbulent wind and irregular wave conditions with U_w=14 m/s, H_s=3.62 m, and T_p=10.29 s, respectively. The responses corresponding to the 2P frequency are observed for each FVAWT. The 2P frequency arises from the characteristic of aerodynamic loads acting on the two-blade VAWT. Since the rotating axis is not parallel to the wind direction, the angle of attack of each

blade varies with the azimuth angle of the shaft, leading to the variation of resulting aerodynamic loads within one revolution. For a two-blade FVAWT, the resultant aerodynamic forces and torque vary twice per revolution and thus give rise to the 2P frequency responses. The semi-submersible FVAWT has larger 2P responses in pitch and roll motions, while the spar FVAWT has large 2P responses in surge and sway motions. These 2P responses increase as the wind speed increases.

Because of the taut mooring system, the spectrum of motions for the TLP FVAWT is much smaller than that of the spar FVAWT and the semi-submersible FVAWT. The surge motions of the three FVAWTs are dominated by the low-frequency responses due to the turbulent wind and surge resonant responses. The wave frequency surge responses are larger than the corresponding 2P responses. The spar FVAWT has much larger wind-induced surge motion, as well as the 2P responses, while the TLP FVAWT has larger wave-frequency surge responses. The spectrum of sway motion differs from the surge spectrum since the wind-induced sway responses of the semi-submersible FVAWT is otherwise much larger than that of the spar FVAWT, though the low-frequency wind-induced sway responses are both dominating,. For the semi-submersible FVAWT, the wind-induced surge and sway are the same order of magnitude, which means that the misaligned wind and wave are of interest, as has been studied by Wang et al. (2015b). The heave spectrum of the three FVAWTs is mainly wave-frequency dominated.

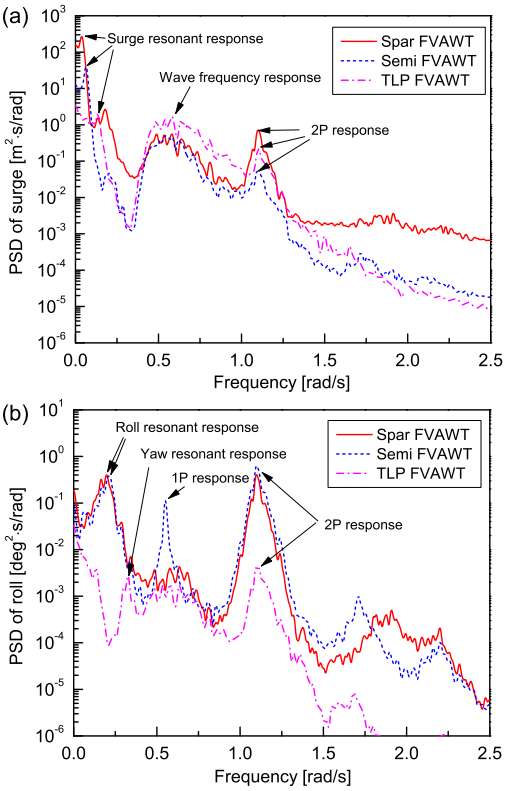

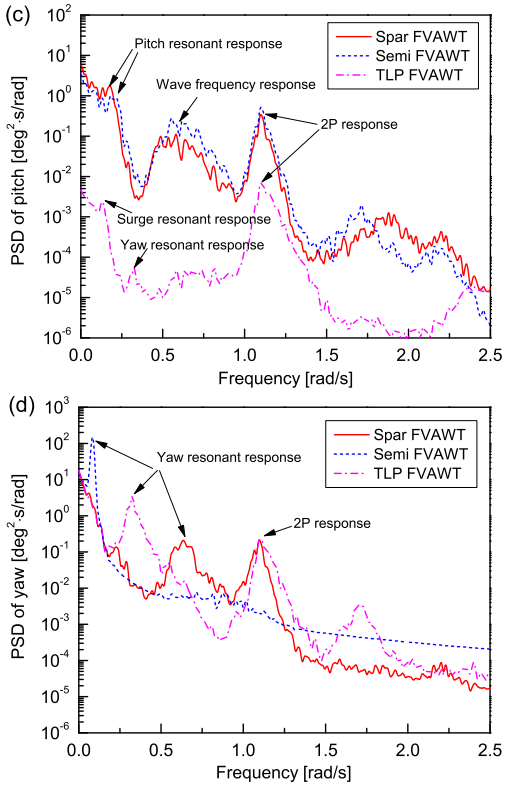

Fig. 6 Power spectra of (a) surge, (b) roll, (c) pitch, and (d) yaw motions for the three FVAWT concepts in LC3.3 with U_w=14 m/s, H_s=3.62 m, and T_p=10.29 s; different scales are used along the abscissa axis and ordinate axis

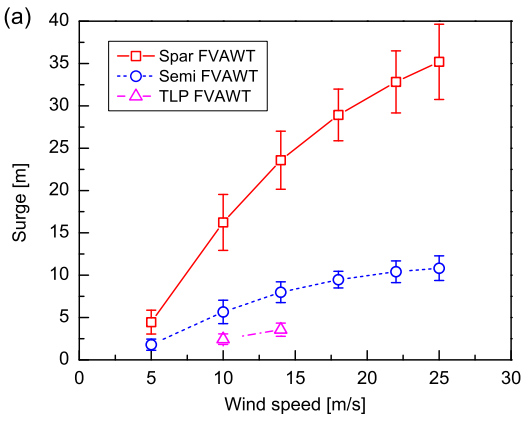

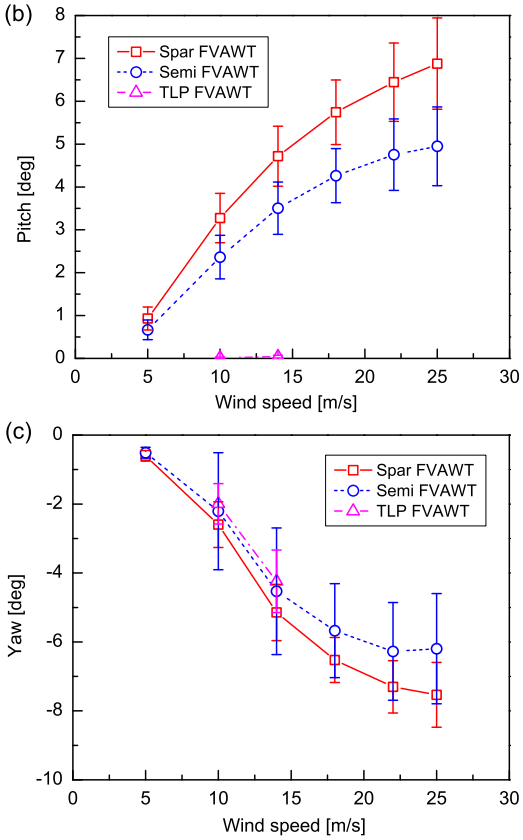

Fig. 7 Mean values of (a) surge, (b) pitch, and (c) yaw motions for the three FVAWT concepts with error bar indicating the standard deviation; there are no results for TLP FVAWT at LC4 through LC6

The spectrum of pitch motions is very similar to that of the surge motion, as the wind-induced responses and the pitch resonant responses are more dominating. The semi-submersible FVAWT has larger wave frequency response and 2P responses in pitch than the spar FVAWT, but the pitch motion of the spar FVAWT is otherwise larger due to the dominating wind-induced responses in the turbulent wind conditions, as shown in Fig. 6(c). The pitch response of the TLP FVAWT is much smaller than the others. Not only the 2P roll response but also the 1P roll response can be observed for the semi-submersible FVAWT, as illustrated in Fig. 6(b). The wind-induced roll responses are very small, which differs from that of sway responses. Regarding the yaw motion, the yaw responses are also dominated by the turbulent wind-induced yaw responses for the three FVAWTs. The yaw motion of the semi-submersible FVAWT is significantly magnified under the turbulent wind condition because the turbulent wind excites the yaw resonant response. For the spar FVAWT and the TLP FVAWT, the 2P yaw response is more prominent than for the semi-submersible FVAWT; this is a consequence of the mooring system used.

Figure 7 compares the mean values and standard deviations of the global motions of the three FVAWT concepts under the turbulent wind and irregular wave conditions. Here only the results of surge, pitch, and yaw motion are presented. The error bar indicates the standard deviation from the mean value. The mean values of the global motion increase as the wind speed increases, since the mean values are mainly wind-induced. For the TLP FVAWT, as a result of the tensioned tendons the vertical motions including the roll, pitch, and heave are close to zero, and the surge and sway are also much smaller than those of the spar FVAWT and the semi-submersible FVAWT. For the spar FVAWT and the semi-submersible FVAWT, the spar FVAWT presents larger mean pitch motion due to the smaller pitch restoring coefficient, but the standard deviations are very close to each other. Since the center of gravity of the spar FVAWT is 73.5 m below MSL, which is much larger than that of the semi-submersible FVAWT, the mean value and standard deviation of surge motion for the spar FVAWT is therefore significantly larger: the mean surge motion reaches 35.20 m under LC3.6. Similar results can be observed for the mean values of roll and sway motions for the spar FVAWT and the semi-submersible FVAWT. Though the mean values of each global motion in surge, sway, pitch, and roll illustrate significant discrepancies for the three FVAWT concepts, the mean yaw motions are fairly close, as shown in Fig. 7(c). In addition, the standard deviation of yaw of the semi-submersible FVAWT is much larger than that of the spar FVAWT: this is because the resonant yaw motions are excited by the turbulent wind.

Tower Base Bending Moment

Here the tower base was assumed to be located below the bearings between the rotating shaft and the drivetrain shaft. The tower base bending moment is caused by the large aerodynamic force acting on the rotor and by the weight of the rotor due to the tower tilt. Even under the same environmental condition, the three FVAWT concepts demonstrate significant differences in platform motions, leading to discrepancies in the tower base bending moment. Here both the tower base fore-aft bending moment M_{FA} and side-to-side bending moment M_{SS} are chosen as the primary structural performance parameters. Since the aerodynamic loads of each blade vary with the azimuthal angle, not only M_{FA} but also M_{SS} have great variations, which is quite different from the HAWT. These variations of bending moments can cause large stress fluctuations, thus leading to great fatigue damage.

Figure 8 compares the power spectra of M_{FA} and M_{SS} under the turbulent wind and irregular wave conditions. The turbulent winds excite the certain low-frequency response of M_{FA}, but the wind-induced response is much smaller than the 2P response in both M_{FA} and M_{SS}. Furthermore, since the taut tendons cannot absorb the 2P aerodynamic excitations for the TLP FVAWT, the 2P responses in M_{FA} and M_{SS} of the spar FVAWT and the semi-submersible FVAWT are much smaller than that of the TLP FVAWT, which implies that the catenary mooring system can greatly mitigate the 2P effects on structural dynamic responses. As a consequence, the standard deviations of M_{FA} and M_{SS} for the spar FVAWT and the semi-submersible FVAWT are smaller than those of the TLP FVAWT, as shown in Fig. 9. Figure 9 compares the mean values and standard deviations of M_{FA} for the three FVAWT concepts under different environmental conditions. The mean values and standard deviations of M_{FA} increase as the wind speed increases. The mean values of M_{FA} for the spar FVAWT and the semi-submersible FVAWT are much larger than the corresponding standard deviations; on the other hand, the standard deviations of the TLP FVAWT are much larger than the mean values. The spar FVAWT has the largest mean value of M_{FA} with smallest standard deviation. A similar effect is also observed for M_{SS} for the three FVAWT concepts.

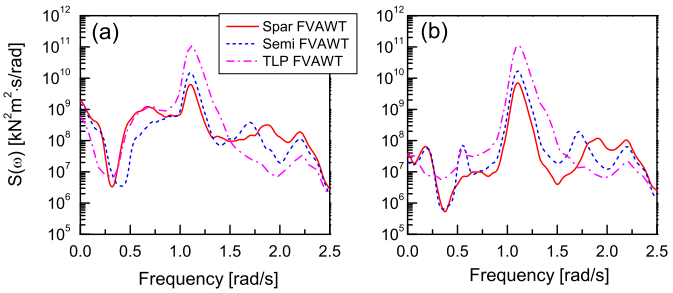

Fig. 8 Power spectra of (a) tower base fore-aft bending moment and (b) tower base side-to-side bending moment for the three FVAWT concepts in LC3.3 with U_w=14 m/s, H_s=3.62 m, and T_p=10.29 s

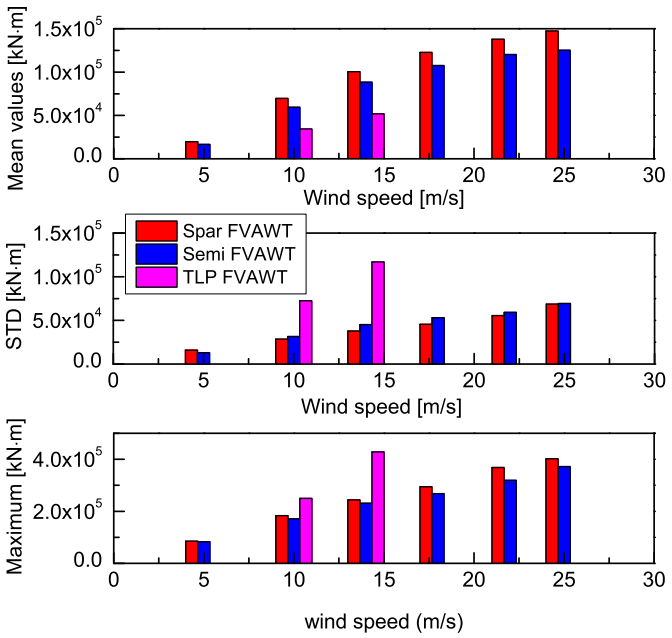

Fig. 9 Mean values, standard deviations, and maximum values of the tower base fore-aft bending moment for the three FVAWT concepts; there are no results for TLP FVAWT at LC4 through LC6

Mooring Line Tension

The mooring system is used to keep the platform in position. Because of the large aerodynamic excitations at high wind speeds, the FVAWT may experience large global motion, especially the yaw motion as shown in Fig. 7(c). The three FVAWT concepts used different mooring systems, as depicted in Fig. 1. The TLP FVAWT employed the three pre-tension tendons, which results in large 2P variation of tension in the tendons, as demonstrated in Fig. 2. The TLP is a desirable supporting structure choice when the variations of the aerodynamic loads acting on the rotor are reduced significantly. This can be achieved by increasing the blade number or using a helical blade (Cahay et al., 2011). One chain mooring system with delta lines and clump weights was applied for the spar FVAWT, and one catenary mooring system was adopted by the semi-submersible FVAWT. In the present study, the mooring line tensions at the fairlead were studied, Fig. 10 presents the power spectrum of the tension of mooring line 2 for the semi-submersible and TLP FVAWTs and delta line 2a for the spar FVAWT under turbulent wind and irregular wave conditions. The mooring lines in the global coordinate system are specified in Fig. 1 for three FVAWT concepts, respectively.

The power spectral density (PSD) of the tension of the TLP FVAWT is approximately three orders of magnitude higher than that of the semi-submersible FVAWT and the spar FVAWT, since the variations of tendon tensions are too large as compared to the other two. For the spar and semi-submersible FVAWTs, the turbulent wind-induced response of the tension of mooring line is dominating, and the contributions from the wave frequency response and 2P response increase as the significant wave height and wind speed increase. Additionally, for the spar FVAWT the delta line tensions are always remaining positive, meaning that the current mooring system is acceptable for the operational condition. Moreover, the mean value, standard deviation, and maximum values of the semi-submersible FVAWT are all larger than that of the spar FVAWT, as shown in Fig. 11.

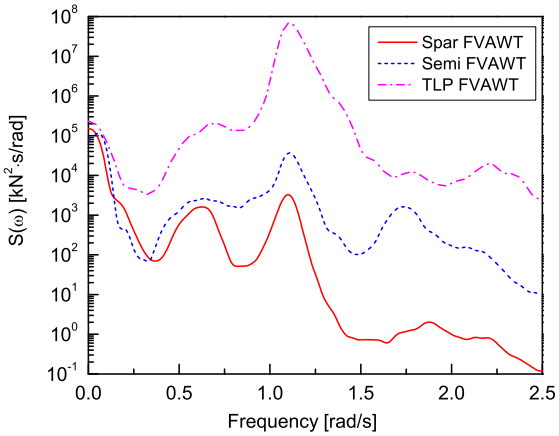

Fig. 10 Power spectrum of the tension in delta line 2a for the spar FVAWT and mooring line 2 for the semi-submersible and TLP FVAWTs in LC3.3 with U_w=14 m/s, H_s=3.62 m, and T_p=10.29 s

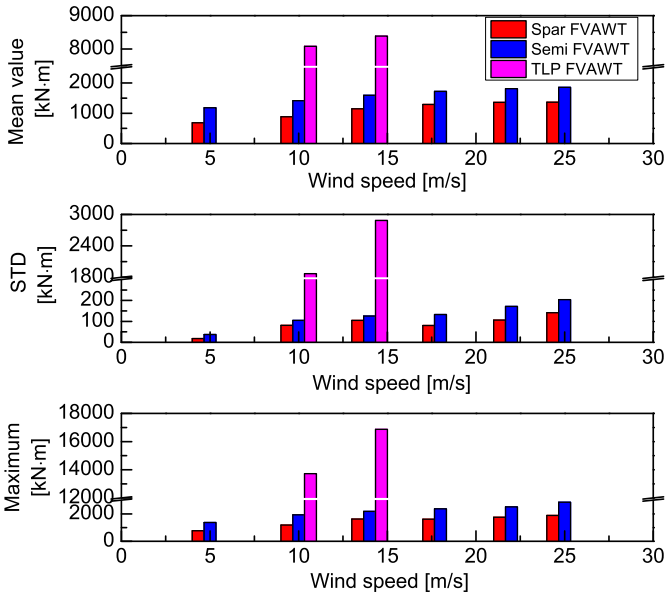

Fig. 11 Mean values, standard deviations, and maximum values of the tension in delta line 2a for the spar FVAWT and mooring line 2 for the semi-submersible and TLP FVAWTs; there are no results for TLP FVAWT at LC4 through LC6

CONCLUSIONS

The present paper deals with a comparative study of the dynamic responses of three FVAWT concepts with a two-bladed Darrieus rotor.

The OC3 spar, the OC4 semi-submersible, and a TLP, which were originally designed to support the NREL 5 MW wind turbine, were taken as the floating platform to support a 5 MW Darrieus rotor. Fully coupled time domain simulations were carried out using the SIMO-RIFLEX-DMS code. A series of load cases with turbulent wind and irregular waves was defined to investigate global stochastic dynamic responses of the three FVAWT concepts, including the generator power production, the platform motions, the tower base bending moment, and the tensions of mooring lines.

Both the mean values and the standard deviations of the generator power production for the three FVAWTs are very close, except that differences in mean power between the spar FVAWT and the semi-submersible FVAWT arise due to the different rotor rotational speeds. For the three FVAWTs, the motion of surge, pitch, and yaw are mainly due to the low-frequency turbulent wind loads, and the responses corresponding to the 2P frequency are observed for each motion. The spar FVAWT suffers the largest mean value and standard deviation of motions in surge, pitch, and yaw. The semi-submersible FVAWT displays the best global motion performance. Though the three FVAWTs experience severe yaw motion, especially at high wind speed, the yaw motion of the semi-submersible FVAWT is mainly caused by the wind-induced yaw resonant response. Attention should be paid to the yaw natural period when designing a semi-submersible for FVAWTs.

Significant 2P effects can be observed in the responses of the tower base bending moments for the three FVAWTs. These 2P responses can cause great fatigue damage and should be reduced, e.g., by damping. The slack mooring lines can mitigate the 2P effects since they are more efficient at absorbing the 2P aerodynamic excitations. In addition, the 2P variations in the aerodynamic loads can be relieved by increasing the number of blades, using helical blades, or adopting more advanced control strategy despite the increasing costs. Large variations of axial force also exist in the tendons of the TLP FVAWT because of the 2P aerodynamic loads. Unless these variations are significantly reduced, the TLP is not a very good supporting structure. The present mooring system with clump weight and delta lines for the spar FVAWT can only work well for the operational condition that a new mooring system is required when extreme condition analysis is carried out. Both the mooring line tensions for the semi-submersible FVAWT and the delta line tensions for the spar FVAWT show an obvious 2P response, but they are much smaller than those for the TLP FVAWT.

Although the three floating platforms are originally designed to support the NREL 5 MW wind turbine, the present study aims to reveal the dynamic response characteristics of each FVAWT concept. The results can help to resolve preliminary design trade-offs among the three FVAWT concepts and will serve as basis for further developments of each FVAWT concept.

ACKNOWLEDGEMENTS

The authors would like to acknowledge financial support from the EU FP7 project MARE WINT (project 309395) through the Centre for Ships and Ocean Structures at the Department of Marine Technology, Norwegian University of Science and Technology, Trondheim, Norway. The first author would also like to thank Dr. Erin Bachynski from MARINTEK for providing the TLP model and kind help with using the simulation codes.

REFERENCES

Bachynski, EE, and Moan, T (2012). "Design Considerations for Tension Leg Platform Wind Turbines," *Marine Struct*, 29(1), 89--114.

Bachynski, EE, Kvittem, MI, Luan, C, and Moan, T (2014). "Wind--Wave Misalignment Effects on Floating Wind Turbines: Motions and Tower Load Effects," *J Offshore Mech Arct Eng*, 136(4), 041902.

Borg, M, and Collu, M (2014). "A Comparison on the Dynamics of a Floating Vertical Axis Wind Turbine on Three Different Floating Support Structures," *Energy Procedia*, 53, 268--279.

Borg, M, Shires, A, and Collu, M (2014). "Offshore Floating Vertical Axis Wind Turbines, Dynamics Modelling State of the Art. Part I: Aerodynamics," *Renewable Sustainable Energy Rev*, 39, 1214--1225.

Cahay, M, Luquiau, E, Smadja, C, and Silvert, F (2011). "Use of a Vertical Wind Turbine in an Offshore Floating Wind Farm," *Offshore Technol Conf*, Houston, Texas, USA, OTC-21705-MS.

Cheng, Z, Wang, K, Gao, Z, and Moan, T (2015). "Comparative Study of Spar Type Floating Horizontal and Vertical Axis Wind Turbines Subjected to Constant Winds," *Proc Eur Wind Energy Assoc Offshore 2015*, Copenhagen, Denmark, EWEA.

Dabiri, JO (2011). "Potential Order-of-Magnitude Enhancement of Wind Farm Power Density via Counter-Rotating Vertical-Axis Wind Turbine Arrays," *J Renewable Sustainable Energy*, 3(4), 043104.

Faltinsen, OM (1995). *Sea Loads on Ships and Offshore Structures*, Cambridge University Press, Cambridge, UK, 340 pp.

IEC (2009). *Wind Turbines, Part 3: Design Requirements for Offshore Wind Turbines,* International Standard 61400-3, International Electrochemical Commission, Geneva, Switzerland.

Islam, MR, Mekhilef, S, and Saidur, R (2013). "Progress and Recent Trends of Wind Energy Technology," *Renewable Sustainable Energy Rev*, 21, 456--468.

Jamieson, P (2011). *Innovation in Wind Turbine Design*, John Wiley & Sons, 316 pp.

Johannessen, K, Meling, TS, and Haver, S (2002). "Joint Distribution for Wind and Waves in the Northern North Sea," *Int J Offshore Polar Eng*, 12(1), 1--8.

Jonkman, BJ (2009). *TurbSim User's Guide: Version 1.50*, Technical Report NREL/TP-500-46198, NREL, Golden, CO, USA.

Jonkman, J (2010). *Definition of the Floating System for Phase IV of OC3*, Technical Report NREL/TP-500-47535, NREL, Golden, CO, USA.

Jonkman, JM, Butterfield, S, Musial, W, and Scott, G (2009). *Definition of a 5-MW Reference Wind Turbine for Offshore System Development*, Technical Report NREL/TP-500-38060, NREL, Golden, CO, USA.

Karimirad, M, and Moan, T (2012). "Wave and Wind Induced Dynamic Response of a Spar-Type Offshore Wind Turbine," *J Waterway Port Coastal Ocean Eng*, 138(1), 9–20.

Kinzel, M, Mulligan, Q, and Dabiri, JO (2012). "Energy Exchange in an Array of Vertical-Axis Wind Turbines," *J Turbulence*, 13(38), 1--13.

Luxcey, N, Ormberg, H, and Passano, E (2011). "Global Analysis of a Floating Wind Turbine Using an Aero-Hydro-Elastic Numerical Model: Part 2, Benchmark Study," *Proc 30th Int Conf Ocean Offshore Arct Eng*, Rotterdam, The Netherlands, OMAE2011-50088.

MARINTEK (2012a). *SIMO-Theory Manual, Version 4.0*.

MARINTEK (2012b). *RIFLEX Theory Manual, Version 4.0*.

Ormberg, H, Passano, E, and Luxcey, N (2011). "Global Analysis of a Floating Wind Turbine Using an Aero-Hydro-Elastic Model: Part 1, Code Development and Case Study," *Proc 30th Int Conf Ocean Offshore Arct Eng*, Rotterdam, The Netherlands, OMAE2011-50114.

Paquette, J, and Barone, M (2012). "Innovative Offshore Vertical-Axis Wind Turbine Rotor Project," *Eur Wind Energy Assoc 2012 Annual Event*, Copenhagen, Denmark, EWEA.

Paraschivoiu, I (2002). *Wind Turbine Design: With Emphasis on Darrieus Concept*, Polytechnic International Press, 438 pp.

Paulsen, US, Pedersen, TF, Madsen, HA, Enevoldsen, K, Nielsen, PH,

Hattel, JH, Zanne, L, Battisti, L, Brighenti, A, and Lacaze, M (2011). "DeepWind: An Innovative Wind Turbine Concept for Offshore," *Eur Wind Energy Assoc 2011 Annual Event*, Brussels, Belgium, EWEA.

Robertson, A, Jonkman, J, Masciola, M, Song, H, Goupee, A, Coulling, A, and Luan, C (2012). *Definition of the Semisubmersible Floating System for Phase II of OC4*, Tech Rep NREL/TP-5000-6060, NREL, Golden, CO, USA.

Vita, L (2011). Offshore Floating Vertical Axis Wind Turbines with Rotating Platform, PhD Report, Technical University of Denmark, Røskilde, Denmark.

Wang, K, Moan, T, and Hansen, MOL (2013). "A Method for Modeling of Floating Vertical Axis Wind Turbine," *Proc 32nd Int Conf Ocean Offshore Arct Eng*, Nantes, France, OMAE2013-10289.

Wang, K, Hansen, MOL, and Moan, T (2015a). "Model Improvements for Evaluating the Effect of Tower Tilting on the Aerodynamics of a Vertical Axis Wind Turbine," *Wind Energy*, 18, 91--110.

Wang, K, Moan, T, and Hansen, MOL (2015b). "Stochastic Dynamic Response Analysis of a Floating Vertical Axis Wind Turbine with a Semi-Submersible Floater," *Wind Energy*, (submitted).

Wang, K, Luan, C, Moan, T, and Hansen, MOL (2014). "Comparative Study of a FVAWT and a FHAWT with a Semi-Submersible Floater," *Proc 24th Int Offshore Polar Eng Conf*, Busan, Korea, ISOPE, 1, 302--310.

Wang, K, Cheng, Z, Moan, T, and Hansen, MOL (2015c). "Effect of Difference-Frequency Forces on the Dynamics of a Semi-Submersible Type FVAWT in Misaligned Wave--Wind Condition," *Proc 25th Int Offshore Polar Eng Conf*, Kona, HI, USA, ISOPE, 1, 517--524.